frontiers | Frontiers in Energy Research

TYPE Original Research
PUBLISHED 31 August 2022
DOI 10.3389/fenrg.2022.987513

OPEN ACCESS

EDITED BY
Jingang Liang,
Tsinghua University, China

REVIEWED BY
Chen Hao,
Harbin Engineering University, China
Donny Hartanto,
Oak Ridge National Laboratory (DOE), United States
Jinsen Xie,
University of South China, China

*CORRESPONDENCE
Wenbin Wu,
wuwb28@mail.sysu.edu.cn

SPECIALTY SECTION
This article was submitted to Nuclear Energy, a section of the journal Frontiers in Energy Research

RECEIVED 06 July 2022
ACCEPTED 08 August 2022
PUBLISHED 31 August 2022

CITATION
Zhong Y, Norman P and Wu W (2022), A feasibility study of SMART reactor power performance optimizations-part 2: Reflector material selection. *Front. Energy Res.* 10:987513. doi: 10.3389/fenrg.2022.987513

A feasibility study of SMART reactor power performance optimizations-part 2: Reflector material selection

Yiming Zhong[1], Paul Norman[1] and Wenbin Wu[2]*

[1]Nuclear Physics Group, School of Physics and Astronomy, College of Engineering and Physical Sciences, University of Birmingham, Birmingham, United Kingdom, [2]Sino-French Institute of Nuclear Engineering and Technology, Sun Yat-sen University, Zhuhai, China

The neutron reflector is a general component in the nuclear reactor design. The original SMART reactor design used light water as a reflector surrounding the fission zone. However, this design has low uranium utilization rates in the outermost fuel assemblies, so poor fuel economy. In this study, six potential reflector materials, i.e., heavy water, graphite, beryllium metal and its oxide, steel, and tungsten carbide has been investigated as the neutron reflector for SMART. Firstly, the materials' cross-sections of neutron scattering and (n, 2n) reactions have been cited from ENDF data libraries and analyzed. This analysis found for the neutrons with energy lower than 1 eV, the ^{9}Be atom has six barn elastic scattering cross-sections, and the ^{9}Be(n, 2n)^{8}Be reaction can compensate for neutron leakage. Then, OpenMC is employed to simulate the effect of these reflector materials on power distribution and depletion. Compared with the original design, the beryllium oxide can improve the initial k_{eff} from 1.22906 to 1.27446, flat the radial direction power distribution. The analysis on both scales agrees that the beryllium oxide is an efficient neutron reflector choice with good material properties.

KEYWORDS

reflector, cross-section, Monte Carlo, power distribution, burn-up

1 Introduction

By analyzing the OpenMC full-core simulation results, the previous study finds low ^{235}U utilization rates in the outside fuel assemblies (FA). The original SMART design uses water surrounding the FAs as the neutron reflector. An efficient reflector can scatter the leaking neutrons back to the core and flat the core radial power distribution (Lamarsh and Baratta, 2001; Stacey, 2018). Due to the smaller size of SMRs' core, the fission-produced neutrons have a higher possibility of entering the reflector than in traditional large PWRs. A crucial factor in determining an integral PWR design's physical viability and fuel economy may be the reflector efficiency. Moreover, the reflector will work in the extensive radiation, high temperature and aggressive chemical environment (Kurosaki and Yamanaka, 2020).

TABLE 1 Material properties of potentially available reflector materials.

Material	Effective isotope	Atomic mass(u)	Melting point (°C)	Density (g/cm^3)
Light water	^{1}H, ^{16}O	1.00784,15.9949	0	0.997
Heavy water	^{2}H, ^{16}O	2.014102,159949	3.81	1.11
Graphite	^{12}C	12	≈3600	2.26
Beryllium	^{9}Be	9.012182	1287	1.85
Beryllium oxide	^{9}Be, ^{16}O	9.012182, 15.9949	2530	3.02
Stainless steel	^{56}Fe	55.93494	1510	7.92
Tungsten Carbide	^{183}W	183.84	2870	15.63

The selection of reflector material would thus somewhat affect the neutronic performance of SMART. In 2015, S. Dawahra's work (Dawahra et al., 2015a) used Monte Carlo N-Particle (MCNP) to study the reflector effect on the IAEA referencing water-moderated material test reactor (IAEA, 1980). The optional fuel enrichments are 20%, 45%, and 93%. Reflectors chosen have light water, heavy water, beryllium and graphite. Similar research was published in 2016. Farrokh Khoshahval (Khoshahval and Salari, 2016) studied the same types of reflector and their effect on the 5MW$_{th}$ pool-type light water Tehran research reactor by WIMS-D4 (Deen et al., 1995) and the CITATION (Fowler and Vondy, 1969) codes. Both works agree that beryllium is a particularly effective reflector material for water-cooled reactors. A later published study investigated the feasibility of replacing Be reflector with its oxide BeO in the miniature neutron source reactor (Dawahra et al., 2015b).

^{9}Be atom will produce neutron from (n, 2n) reaction. If the neutron is in the fast energy range, ^{9}Be will produce helium and tritium in the (n, α) reaction. Some USA studies have investigated the beryllium reflector and its composition effect on the research reactors (Ilas, 2013; Puig and Dennis, 2016). The depletion of pre-existing impurities will significantly affect reactivity. Besides the water reactors, researchers also propose using the beryllium-based material in the high-temperature gas-cooled reactor (HTGR). S. Atkinson performed studies (Atkinson et al., 2019) that compared beryllium oxide and nuclear graphite as TRISO fuel containers and reflectors for HTGR U-Battery.

In the PWR design, the vertical and horizontal plates form a supportive component called the assembly baffle, which is the interface between the core and the reactor barrier (Bosch et al., 2021; Ge´rard and Somville, 2009). Generally, there is water between the baffle and core barrier. On the other hand, some

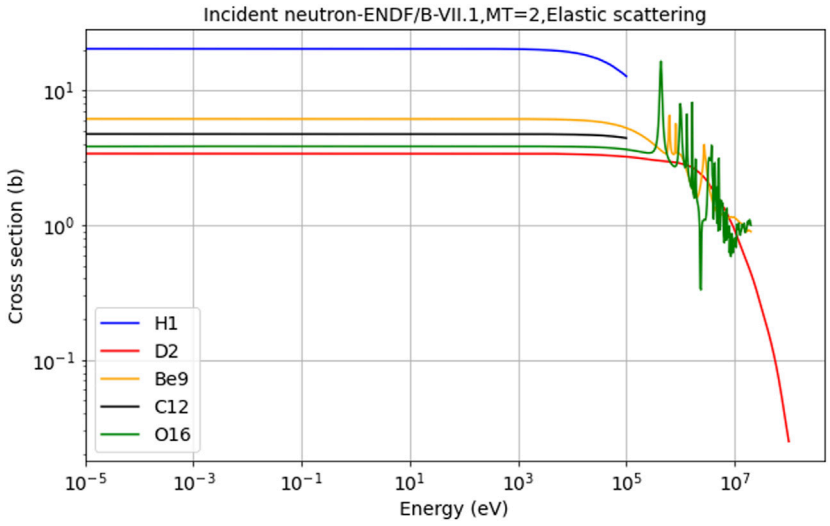

FIGURE 1
Elastic scattering cross-sections (0k) of ^{1}H, ^{2}H, ^{9}Be,^{12}C,^{16}O versus incident neutron energy.

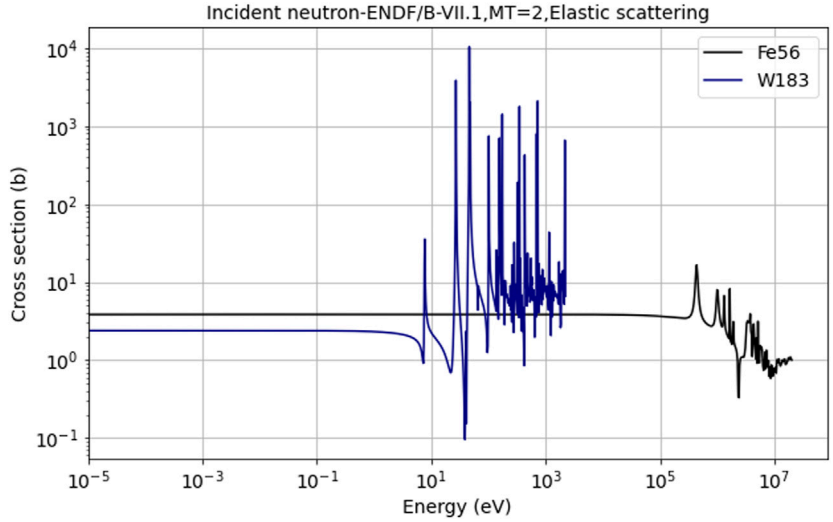

FIGURE 2
The elastic scattering cross-section (0k) of heavy atomic mass isotopes ^{56}Fe, ^{183}W.

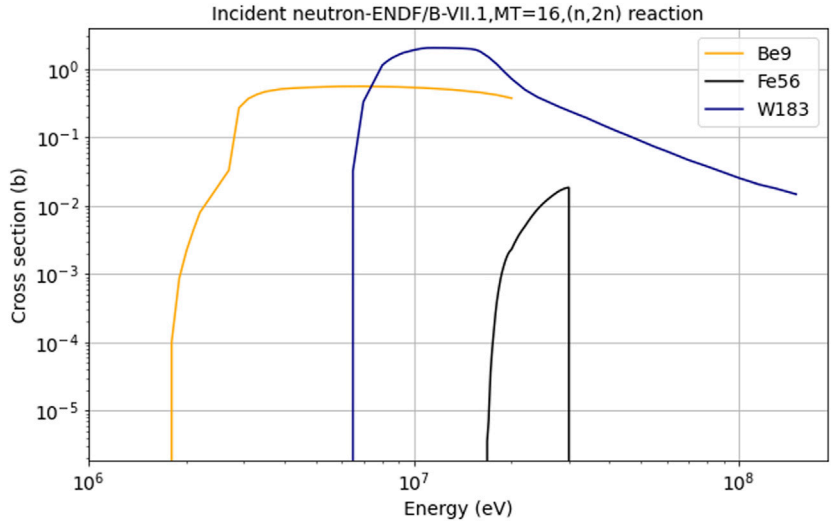

FIGURE 3
(n, 2n) reaction, MT = 16 cross-section distributions of ^{9}Be, ^{56}Fe, ^{183}W.

institutes study the feasibility of heavy material reflectors, like stainless steel walls surrounding the core (Czakoj et al., 2022). Košťál' experiment confirms the strong neutron-absorbing effect from the VVER-1000 (Vojackova et al., 2017) heavy reflector' cooling channel water. The related research has already been done by both deterministic and Monte Carlo codes (Sargeni et al., 2016; Taforeau et al., 2019). Sargeni's work focus on core power tilt. This asymmetry problem was first studied by the diffusion code CRONOS2 (Lautard et al., 1992) and then benchmarked by MCNP. In addition, some small integral PWRs inherit technology from large reactors designs with steel reflectors, such as I^{2}S-LWR (Flaspoehler and Petrovic, 2020) and IRIS(Carelli et al., 2004). Besides, some studies are trying to replace the water in the baffle with other light materials such as graphite and beryllium in the long life-cycle small water coolant designs (Bae and Hong, 2015; Wankui et al., 2017).

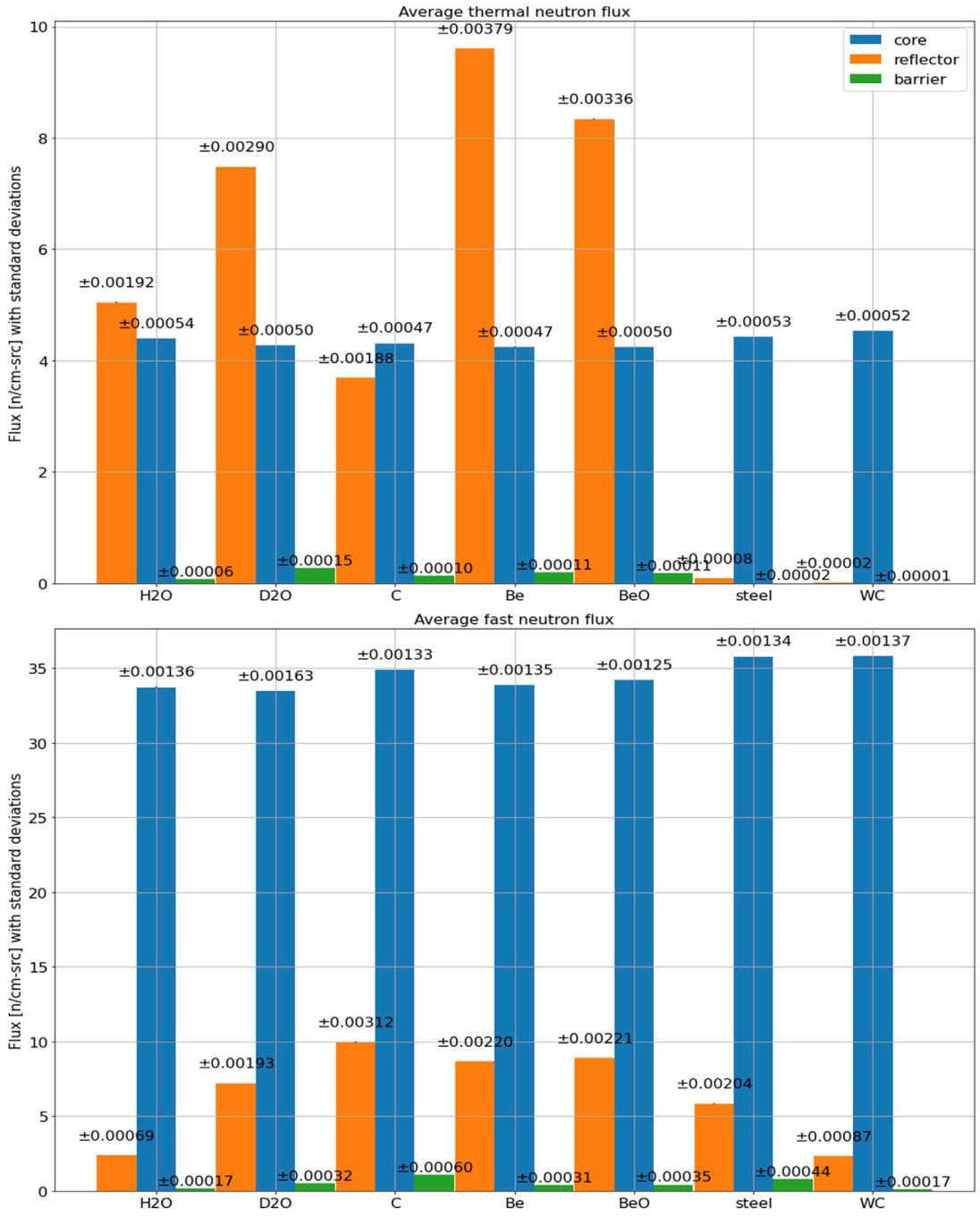

FIGURE 4
Bar charts of thermal and fast neutron flux with standard deviations for core, reflector and barrier.

The author's previous study builds and validates an OpenMC (Romano et al., 2015) SMART full reactor core model with a two-batch refuelling fuel layout (Choi, 2015). The supplementary material section will remind the schematic of this model. This work will first analyze the reflector materials' neutron reaction cross-sections. Then, filling the selected materials into the model's reflector cell in sequence to simulate the reflected-core power performances. Meanwhile, the simulation process acquires the corresponding reaction rates and k_{eff} eigenvalues. The simulation and analysis results will determine the suitable reflector material for SMART.

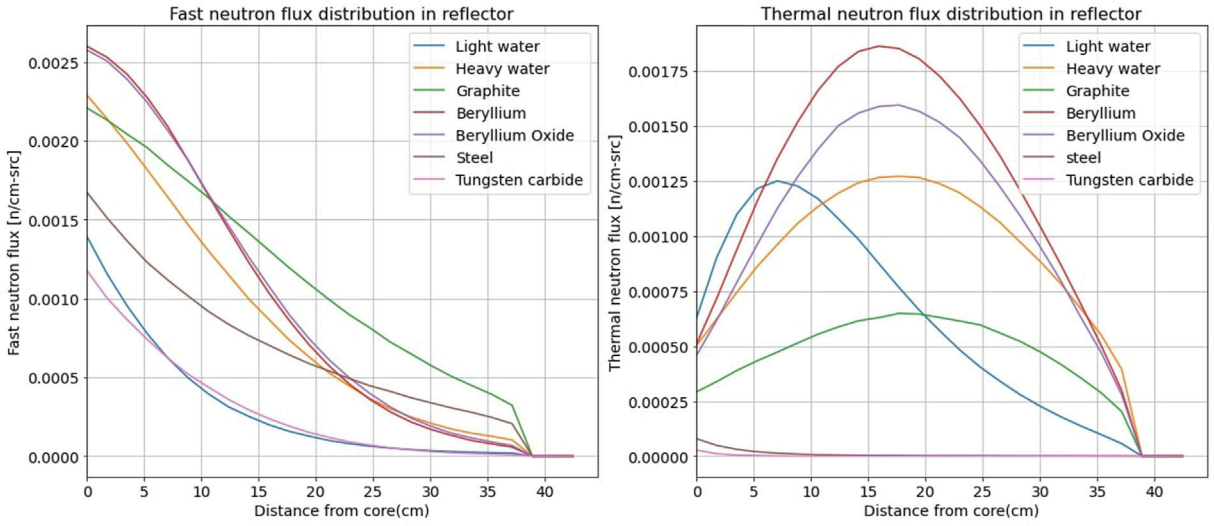

FIGURE 5
Values of neutron flux versus the distance away from FA boundaries.

2 Reflector material

A suitable moderator material is also an acceptable reflector material because of its low absorption cross-section σ_a and high scattering cross-section σ_s. According to the published literature and technical reports, the author selected potential light atomic mass reflector materials such as heavy water, graphite, beryllium, beryllium oxide, and a couple of heavy metal materials: stainless steel and tungsten carbide. Besides these, the water itself is a commonly applied reflector material. Heavy water D_2O and graphite are widely used materials in nuclear reactor designs. Several PWRs utilize heavy water as primary circle coolant and moderator, such as CANDU reactor (Torgerson et al., 2006) from Canada, and IPHWR-700 (Bhadauria et al., 2021) from India.

Many high operating temperature reactor designs use graphite as the moderator, just like the United Kingdom's advanced gas-cooled reactors (AGR). The recently developed pebble-bed HTGR (Zhang et al., 2016) also use graphite to contain TRISO fuel particles. The beryllium-based materials were studied for space reactors due to their low density and outstanding thermal performance (Snead and Zinkle, 2005). The melting points are 1287°C and 2530°C, and thermal conductivities are 200 W m^{-1} K^{-1} (300 K) and 281 W m^{-1} K^{-1} (293 K) for beryllium metal and beryllium oxide, respectively. The neutron irradiation will give negative feedback to the thermal conductivities (Kurosaki and Yamanaka, 2020). Beryllium does not react with water or steam. However, BeO is expensive and toxic. Fabricating metal beryllium with BeO or $Be(OH)_2$ makes it more costly. Therefore, applying beryllium reflectors in SMART should consider the material economy and cost.

Usually, Heavy metal materials are difficult to slow down neutrons, but they can shield the radiation from the core. The application of stainless steel as a neutron reflector has been well studied (Frybort et al., 2020). Tungsten carbide (WC) has a very high melting point at 2870°C, which was a neutron reflector for a nuclear weapon in the early stage of nuclear power development. Meanwhile, tungsten carbide is considered a novel shielding material for SMRs due to its high densities and fast neutron capture cross-section (Giménez and Lopasso, 2018). Similar to beryllium, WC also does not react with water. The material properties of these materials are summarized in Table 1.

The particular reactions' cross-sections have been collected from IAEA evaluated data libraries ENDF for each material (Brown et al., 2018). The OpenMC code reserves a data process Python package. The essential function is analyzing and converting nuclear data from the ACE files and generating libraries in the HDF5 format for the transport solver. In an ENDF dataset, the data would be parameterized by the model calculations and reduced to a tabular form.

3 Results and discussion

3.1 Nuclear data analysis

3.1.1 Elastic scattering

Figure 1 gives the elastic cross-sections for the light atomic isotopes in Table 1. The five isotopes all have possibilities for elastic neutron scattering. For neutrons with energy lower than 1 eV, the cross-section of ^{1}H is 20 b. For ^{2}H, ^{9}Be, and ^{12}C, there are 3.39, 6.15 and 4.75 b. The cross-section values would decrease

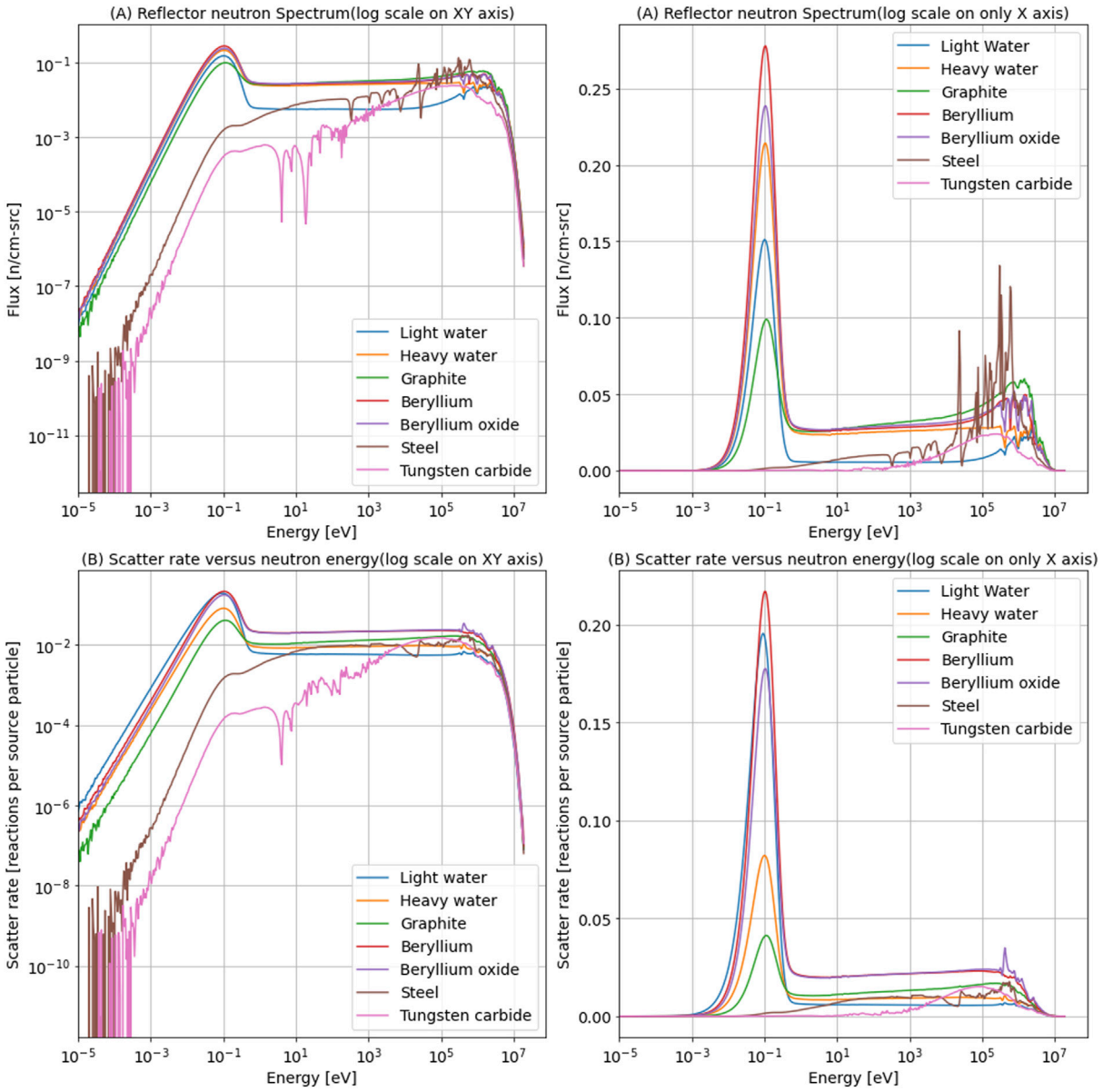

FIGURE 6
The incident neutron energy spectra and scattering reaction energy distributions within reflector materials.

when the incident neutrons speed up. However, they still have the probability of slowing down the fast neutrons. ^{16}O isotope also has a significant elastic scattering cross-section to incident neutrons, and its distribution exists a significant oscillation between the energy range from 10^5–10^7 eV.

Figure 2 gives the resolved resonance energy range elastic scattering cross-section distributions of heavy atomic mass isotopes ^{56}Fe and ^{183}W. In this region, the experimental resolution is enough to observe the resonance and determine its parameters. The sensitivity area of ^{56}Fe is between 10^5 and 10^7 eV. For the lower energy incident neutrons, its σ_s are small than Be^9, about 3.842 b.

3.1.2 (n, 2n) reaction

This study also investigates the potential (n, 2n) reactions. Beryllium can be a neutron multiplier due to the ^{9}Be(n,2n)^{8}Be reaction. Checking the ENDF files of the potential reflector materials, the rich neutron isotopes ^{56}Fe and ^{183}W also have probabilities for (n, 2n) reactions. Their cross-section distributions have been

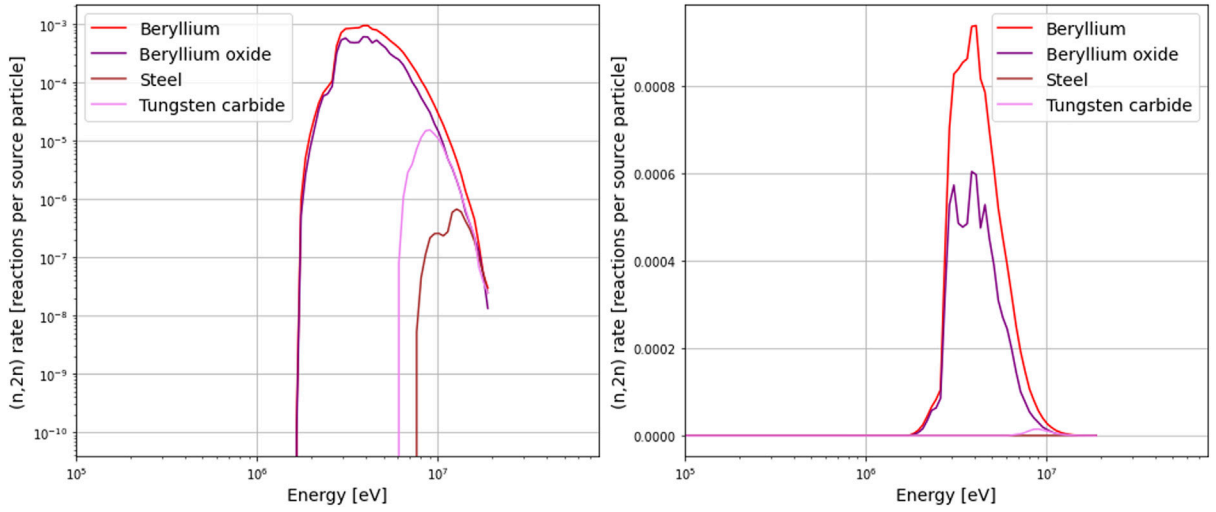

FIGURE 7
The (n, 2n) reaction rate distributions versus incident neutron energy.

TABLE 2 The total scattering rate and absorption rate of reflector materials (units: reactions per source particle).

Reflector materials	Scatter (mean)	Std. dev	Absorption (mean)	Std. dev
Light water	8.829	0.003	0.04862	2×10^{-5}
Heavy water	5.456	0.002	4.81×10^{-4}	3.1×10^{-7}
Graphite	5.116	0.002	8.46×10^{-4}	5.1×10^{-7}
Beryllium	13.34	0.004	0.01194	4×10^{-6}
Beryllium oxide	12.14	0.0036	0.0075	2×10^{-6}
Steel	2.484	0.001	0.0212	1.1×10^{-5}
Tungsten carbide	1.505	0.0006	0.04542	2×10^{-5}

TABLE 3 k_{eff} eigenvalue results of two-batch refuelling scheme core with different material reflectors.

Material	k_{eff}
Light water	$1.22906 \pm 7 \times 10^{-5}$
Heavy water	$1.25921 \pm 7 \times 10^{-5}$
Graphite	$1.25157 \pm 7 \times 10^{-5}$
Beryllium	$1.27613 \pm 7 \times 10^{-5}$
Beryllium oxide	$1.27446 \pm 6 \times 10^{-5}$
Steel	$1.22754 \pm 6 \times 10^{-5}$
Tungsten carbide	$1.21344 \pm 7 \times 10^{-5}$

plotted in Figure 3. The incident neutron must be higher than a particular energy threshold to induce an (n, 2n) reaction.

The ^{9}Be atom has an (n, 2n) reaction threshold of 1.8 MeV. That cross-section would be higher than 0.27 b and stay stable when neutron energy is over 2.9 MeV. Heavy isotope ^{183}W's cross-section is significant for fast energy neutrons, $\sigma_{n,2n}$ is bigger than 2 b for the neutron in the energy range 11–14 MeV. However, $\sigma_{n,2n}$ will decrease lower than 1 b if the incident neutron energy exceeds 19 MeV.

The nuclear data studies in this work are helpful in qualitatively selecting the proper reflector material. However, due to the difference in material densities, the number of isotope atoms in particular geometry spaces would significantly differ. Only comparing the cross-section data could not give reasonable results.

3.2 Reflected core simulation

The simulations record the average flux values of core, reflector and barrier three cells to evaluate the effect of reflectors. Supplementary Figure S1 presents the cells' spatial

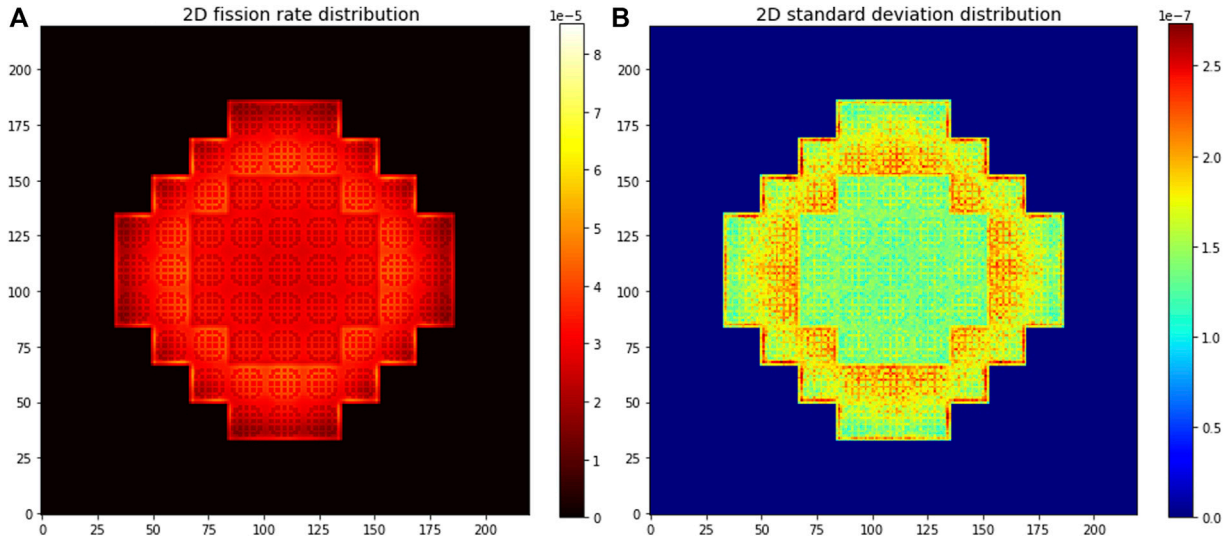

FIGURE 8
Fission rate and standard deviation distributions of two-batch refuelling scheme core with light water reflector.

positions, and this figure also shows how the model is divided into the twelve spatial burn-up zones. The simulations in the following section adopt the operating temperature condition and 0.7 g/cm^3 expanded water density. Figure 4 uses bar height to present the flux values.

For the core, the average fast and thermal neutron flux values are generally close, whatever the reflector material type is. The difference between the maximum and minimum fast neutron flux is 2.1 n/cm-src, and for thermal neutron flux, it is 0.2 n/cm-src. On the contrary, reflector cells' flux values have apparent differences in both energy groups.

The Be metal reflector has the highest average thermal neutron flux, 9.6105 n/cm-src, and the second one is in BeO, 8.3436 n/cm-src. Heavy materials have two orders of magnitude less thermal neutron flux than light materials. For the fast neutrons, its maximum flux is in the graphite reflector. The green bars represent the neutron flux in the steel barrier that should not be neglected. Steel and WC block the most thermal neutrons from getting into the barrier. However, the steel cannot effectively function to shield the fast neutrons. 0.7658 n/cm-src is the most significant remaining fast neutron flux value after the reflection and shield in all simulations.

The neutron flux spatial distribution in particular material reflectors also have been investigated. The reflector geometry in this study is constant. The spatial distribution results can provide a meaningful reference to determine the size of the reflector made by a particular material.

The curves in Figure 5 represent the neutron flux fluctuations in the reflector along the model's diagonal. Four light mass materials and steel reflectors improve the fast neutron flux values near the boundary. The beryllium-based materials give the most significant improvements. Fast neutron moderation in different media produces a series of thermal neutron flux peaks. The thermal neutron flux peak in light water is closer to the boundary than in other light mass reflectors.

The isotopes' cross-section for a particular reaction depends on the incident neutron energy at a specific temperature. Figure 6 shows several tallied reflectors' neutron energy spectra. The plots in Figure 6 could be seen as a supplement to explain the results in Figure 4. The neutron flux integrations are now represented in the energy spaces. The simulations also record the scattering reaction rate and corresponding incident neutron energy.

Observing the spikes located at 10^{-1} eV in Figures 6A,B, the neutron flux in light water is lower than that in heavy water. However, the neutron scattering rate is higher. The beryllium metal reflector has the most significant scattering reaction rate for all energy ranges. When neutron energy is around 10^{-1}eV, the scattering ability of BeO is weaker than light water and beryllium metal. The neutron energy increase will enhance the BeO's reflection ability. The scattering reaction diagrams of Be-based materials overlap, only having a few variances when neutron energy is between 10^5 and 10^6. Meanwhile, the absorption rates have also been recorded in these simulations. Table 2 presents the tally results.

The results in Table 2 show hydrogen atom has a high elastic scattering cross-section but do not have the best reflection ability. The neutron absorption rate of light water is the highest of all potential materials. The (n, 2n) reactions in the materials related to Figure 3 have also been recorded through the simulations. In Figure 7, the beryllium-based materials have much higher possibilities than metal materials to compensate for neutrons by (n, 2n) reaction. The integrated (n, 2n) reaction rates for Be and BeO are $0.013964 \pm 9 \times 10^{-6}$ and $0.009414 \pm 7 \times 10^{-6}$. For steel and tungsten carbide are $0.001803 \pm 1 \times 10^{-6}$ and $0.001924 \pm 2 \times 10^{-6}$.

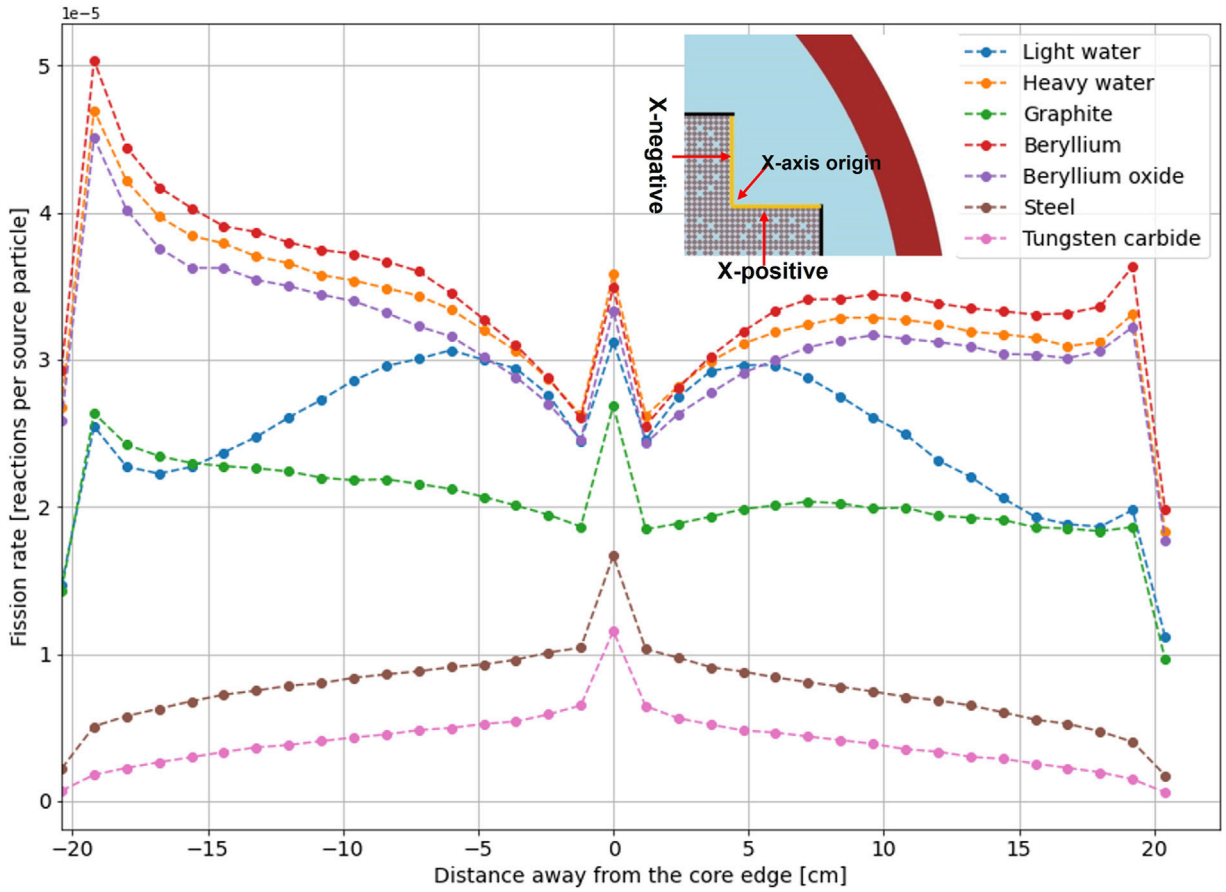

FIGURE 9
Fission rates among the boundary between the fuel assembly and reflector.

Considering that the above-mentioned neutron incident reactions are dispersed, the full-core criticality results are presented in Table 3, which are obtained from material-specific reflective core model simulations.

The variation of k_{eff} represents the upgrade to reactivity from the different reflectors. The beryllium- based materials' reflector gives an extra 4540 pcm improvement. The heavy water and graphite promote the k_{eff} from 1.22907 to a level higher than 1.25, and the enhancement from heavy water is slightly more substantial than graphite. The initial k_{eff} values of heavy metal reflective models are even lower than the original design. The power distributions of different material reflected core have been tallied.

Figure 8 states the fission reaction rate and the associated standard deviation 2D distributions over the entire two-batch refuelling scheme core with the light water reflector. The average fission rate is high in the higher enrichment fuel assembly area and surrounding the reloading fuels. Besides, it can find the power peak along the boundary between the fuel assemblies and reflector. The boundary fission rates also have higher standard deviations. Similar to Figure 8A, the fission rate distributions of other materials reflected models are plotted and combined in one figure. The results will give in Supplementary Figure S2. The scales in these distribution graphs are normalized to show the differences.

To further observe the power peaking on the boundary induced by the proposed reflectors, the tilled fission reaction rates along a characteristic edge are picked up from each distribution graph and plotted in Figure 9. Its legend demonstrates the vertex position and sets it as the origin on the X-axis. The distance along borders express as X-axis' positive and negative values. The selected edge is also highlighted in Supplementary Figure S1. Heavy water brings the most significant effect to the edge vertex in all potential reflectors. However, its improvement for the assembly border is not as substantial as the beryllium reflector. The graphite, steel and tungsten carbide reflectors decrease the original design's boundary power peak and flat the fission rate drops.

The burn-up calculations of reflected-core models also have been done. The k_{eff} value variations of each analysis have been plotted in Figure 10. Compared with the originally designed water reflected core, the aforementioned four types of light materials reflector all improved their depletion diagrams to a

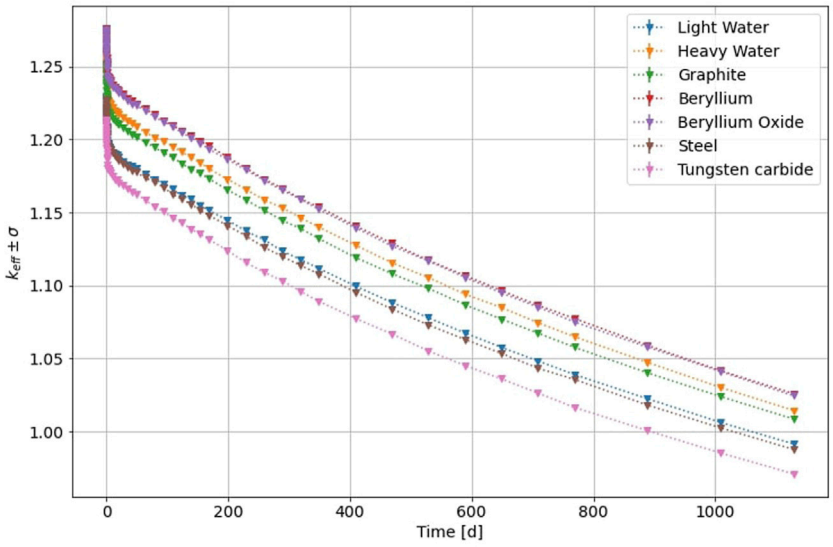

FIGURE 10
The comparison between k_{eff} variations of normal SMART with different reflector materials.

TABLE 4 The k_{eff} values at the beginning and end of the cycle in each of the depletion calculations.

Reflector materials	k_{eff} (BOC)	k_{eff} (EOC)	Depleted reactivity (pcm)
Light water	$1.22957 \pm 32 \times 10^{-5}$	$0.99136 \pm 34 \times 10^{-5}$	23821
Heavy water	$1.25926 \pm 34 \times 10^{-5}$	$1.01431 \pm 34 \times 10^{-5}$	24495
Graphite	$1.25190 \pm 33 \times 10^{-5}$	$1.00848 \pm 30 \times 10^{-5}$	24342
Beryllium	$1.27581 \pm 33 \times 10^{-5}$	$1.02580 \pm 34 \times 10^{-5}$	25001
Beryllium oxide	$1.27526 \pm 34 \times 10^{-5}$	$1.02438 \pm 32 \times 10^{-5}$	25088
Steel	$1.22751 \pm 37 \times 10^{-5}$	$0.98760 \pm 29 \times 10^{-5}$	23991
Tungsten carbide	$1.21310 \pm 36 \times 10^{-5}$	$0.97092 \pm 29 \times 10^{-5}$	24218

higher level, which have EOC k_{eff} higher than 1. The depletion diagrams of beryllium-based material reflector cores always stay at the top of the figure during the whole burn-up process. The depleted reactivity are given in Table 4.

According to the above analysis, the appearance of beryllium-based material reflectors can bring maximum extra reactivity. Therefore, from the neutronic point of view, the beryllium-based materials could be ideal for SMART neutron reflectors to optimize the power output and distribution.

4 Conclusion

The neutron reflectors improve the fission rate and uranium utilization of the outer SMART core FAs. It then optimizes the general power distribution and performance of the SMART design. The simulation results with the selected reflectors show that the light material group could improve the k_{eff}. The improvements from beryllium-based materials are the most significant in this study. In the same depletion period, these two material reflectors let SMART core depletes extra 1180 and 1267 pcm reactivity. The heavy metal reflectors do not bring the extra reactivity in the simulations, and the steel reflector does not shield as much neutron radiation as tungsten carbide. According to the analysis results, the beryllium-based materials are ideal materials for SMART to optimize power performance. Moreover, beryllium oxide has better material properties than its pure metal, such as a higher melting point, reasonable thermal conductivity, and no demand for the individual production process. The future studies will adopt the BeO-reflected core model to investigate the optimized fuel layouts with less fresh fuel demand in the beginning of cycle, and a sustainable refuelling strategy.

Data availability statement

The raw data supporting the conclusion of this article will be made available by the authors, without undue reservation.

Author contributions

All authors contributed to the writing and reviewing of the manuscript. YZ contributed to the modelling and data analysis. All studies are under the guidance and supervised by PN. WW organized the paper publication process.

Conflict of interest

The authors declare that the research was conducted in the absence of any commercial or financial relationships that could be construed as a potential conflict of interest.

Publisher's note

Supplementary material

The Supplementary Material for this article can be found online at: https://www.frontiersin.org/articles/10.3389/fenrg.2022.987513/full#supplementary-material

SUPPLEMENTARY FIGURE S1
OpenMC full core model with two-batch refuelling scheme and twelve burn-up zones spatial division.

SUPPLEMENTARY FIGURE S2
Power distributions of two-batch refuelling scheme core with particular material reflectors.

References

Atkinson, S., Abram, T. J., Litskevich, D., and Merk, B. (2019). Small modular high temperature reactor optimisation – Part 1: A comparison between beryllium oxide and nuclear graphite in a small scale high temperature reactor. *Prog. Nucl. Energy* 111, 223–232. doi:10.1016/j.pnucene.2018.10.017

Bae, G., and Hong, S. G. (2015). A small long-cycle PWR core design concept using fully ceramic micro-encapsulated (FCM) and UO2–ThO2 fuels for burning of TRU. *J. Nucl. Sci. Technol.* 52, 1540–1551. doi:10.1080/00223131.2015.1018364

Bhadauria, M., Kumar, R., and Das, A. K. (2021). Design and investigation of weight bundle simulator for Indian phwr using apdl-a thermal aspect, *EPJ web of conferences. EDP Sciences* 247, 06042.

Bosch, R. W., Van Renterghem, W., Van Dyck, S., Chaouadi, R., Gérard, R., and Somville, F. (2021). Microstructure, mechanical properties and IASCC susceptibility of stainless steel baffle bolts after 30 years of operation in a PWR. *J. Nucl. Mater.* 543, 152615. doi:10.1016/j.jnucmat.2020.152615

Brown, D. A., Chadwick, M. B., Capote, R., Kahler, A. C., Trkov, A., Herman, M. W., et al. (2018). ENDF/B-VIII.0: The 8th major release of the nuclear reaction data library with CIELO-project cross sections, new standards and thermal scattering data. *Nucl. Data Sheets* 148, 1–142. doi:10.1016/j.nds.2018.02.001

Carelli, M. D., Conway, L. E., Oriani, L., Petrović, B., Lombardi, C. V., Ricotti, M. E., et al. (2004). The design and safety features of the IRIS reactor. *Nucl. Eng. Des.* 230, 151–167. doi:10.1016/j.nucengdes.2003.11.022

Choi, S. (2015). "Small modular reactors (SMRs): The case of the Republic of Korea," in *Handbook of small modular nuclear reactors* (Woodhead Publishing Limited). doi:10.1533/9780857098535.4.379

Czakoj, T., Schulc, M., Šimon, J., Jur, V., Košt, M., Ulmanová, J., et al. (2022). The effect of heavy reflector on neutronic parameters of core. *Ann. Nucl. Energy* 168, 108898. doi:10.1016/j.anucene.2021.108898

Dawahra, S., Khattab, K., and Saba, G. (2015b). Investigation of BeO as a reflector for the low power research reactor. *Prog. Nucl. Energy* 81, 1–5. doi:10.1016/j.pnucene.2014.12.001

Dawahra, S., Khattab, K., and Saba, G. (2015a). Study the effects of different reflector types on the neutronic parameters of the 10 MW MTR reactor using the MCNP4C code. *Ann. Nucl. Energy* 85, 1115–1118. doi:10.1016/j.anucene.2015.07.029

Deen, J. R., Woodruff, W. L., and Costescu, C. I. (1995). *WIMS-D4M user manual.* doi:10.2172/197846

Flaspoehler, T., and Petrovic, B. (2020). Radiation environment in the I2S-lwr concept: Part I – radial distribution and its impact on vessel fluence, neutron detectors placement, and radial reflector gamma heating. *Ann. Nucl. Energy* 145, 106272. doi:10.1016/j.anucene.2018.07.021

Fowler, T. B., and Vondy, D. R. (1969). *Nuclear reactor core analysis code: Citation.*

Frybort, J., Sklenka, L., Fejt, F., Suk, P., and Frybortova, L. (2020). Sensitivity analysis of stainless steel reflector for VR-1 training reactor. *EPJ Web Conf.* 247, 08003. Int. Conf. Phys. React. Transit. to a Scalable Nucl. Futur. PHYSOR 2020 2020-March, 1578–1585. doi:10.1051/epjconf/202124708003

Ge´rard, R., and Somville, F. (2009). "Situation of the baffle-former bolts in Belgian units," in *International conference on nuclear engineering* 43512, 521–528.

Giménez, M. A. N., and Lopasso, E. M. (2018). Tungsten carbide compact primary shielding for small medium reactor. *Ann. Nucl. Energy* 116, 210–223. doi:10.1016/j.anucene.2018.02.032

IAEA (1980). *Research reactor core conversion from the use of highly enriched uranium fuels: Guidebook, TECDOC series.* Vienna: International Atomic Energy Agency.

Ilas, D. (2013). Impact of HFIR LEU conversion on beryllium reflector degradation factors. *Oak Ridge National Laboratory.*

Khoshahval, F., and Salari, F. (2016). Sensitivity analyses of the use of different reflector materials on the neutronics parameters of Tehran research reactor. *Prog. Nucl. Energy* 93, 351–361. doi:10.1016/J.PNUCENE.2016.09.009

Kurosaki, K., and Yamanaka, S. (2020). "7.12 - neutron reflector materials (Be, hydrides)," in *Comprehensive nuclear materials*. Editors R. J. M. Konings and R. E. Stoller. Second Edition (Oxford: Elsevier), 382–399. doi:10.1016/B978-0-12-803581-8.11747-3

Lamarsh, J. R., and Baratta, A. J. (2001). *Introduction to nuclear engineering.* Saddle River, NJ: Prentice hall Upper.

Lautard, J. J., Loubière, S., and Fedon-Magnaud, C. (1992). CRONOS: A modular computational system for neutronic core calculations. *IAEA-TECDOC.*

Puig, F., and Dennis, H. (2016). Neutron fluence effects on SLOWPOKE-2 beryllium reflector composition and reactivity. *Nucl. Eng. Des.* 305, 451–460. doi:10.1016/j.nucengdes.2016.05.033

Romano, P. K., Horelik, N. E., Herman, B. R., Nelson, A. G., Forget, B., and Smith, K. (2015). OpenMC: A state-of-the-art Monte Carlo code for research and development. *Ann. Nucl. Energy* 82, 90–97. doi:10.1016/j.anucene.2014.07.048

Sargeni, A., Burn, K. W., and Bruna, G. B. (2016). The impact of heavy reflectors on power distribution perturbations in large PWR reactor cores. *Ann. Nucl. Energy* 94, 566–575. doi:10.1016/j.anucene.2016.03.015

Snead, L. L., and Zinkle, S. J. (2005). Use of beryllium and beryllium oxide in space reactors. *AIP Conf. Proc.* 746, 768–775. doi:10.1063/1.1867196

Stacey, W. M. (2018). *Neutron energy distribution. Nuclear reactor physics*. 3rd Edn.Wiley VCH Verlag GmbH & Co. KGaA (Wiley Online Books).

Taforeau, J., Muller, M., and Salino, V. (2019). Modeling of heavy reflectors using DONJON-5. *Ann. Nucl. Energy* 127, 319–325. doi:10.1016/J.ANUCENE.2018.12.017

Torgerson, D. F., Shalaby, B. A., and Pang, S. (2006). CANDU technology for Generation III+ and IV reactors. *Nucl. Eng. Des.* 236, 1565–1572. doi:10.1016/j.nucengdes.2006.04.020

Vojackova, J., Novotny, F., and Katovsky, K. (2017). Safety analyses of reactor VVER 1000. *Energy Procedia* 127, 352–359. doi:10.1016/j.egypro.2017.08.079

Wankui, Y., Songbao, Z., Yaoguang, L., Weili, N., and Li, D. (2017). Neutron fluence analysis of graphite reflector in SPRR-300 during the whole reactor lifetime. *Ann. Nucl. Energy* 106, 91–96. doi:10.1016/j.anucene.2017.03.046

Zhang, Z., Dong, Y., Li, F., Zhang, Z., Wang, H., Huang, X., et al. (2016). The shandong shidao bay 200 MWe high-temperature gas-cooled reactor pebble-bed module (HTR-PM) demonstration power plant: An engineering and technological innovation. *Engineering* 2, 112–118. doi:10.1016/J.ENG.2016.01.020